CHAPTER 6

Analytical Study

6.1 Numerical simulation result and verification and discussions

The FE models were first validated by comparison with the experimental study by using the backbone curves and hysteretic responses, as shown in Figures. 6.1 to 6.7. The initial stiffness matched quite well. However, there is a small difference in the backbone curves after the peak load. The ultimate loads from the numerical results were compared with the experimental results. As shown in Table 6.1, the numerical results were in good agreement, even though the FE maximum strength was slightly different compared to the experimental results. The comparisons indicated that the fiber based FE model developed through the SeismoStruct 2016 with the proposed FE modelling successfully predicted the ultimate load capacity, hysteretic response, and relationship of the lateral story shear versus the lateral displacement.

Table 6.1 Comparison of experimental and FEM results

Ultimate Load ,H (kN)	FE	EXP	FE/EXP
M1 (Push/Pull)	42.20/42.06	44.43/42.08	0.95/1.00
P1 (Push/Pull)	36.99/30.99	36.49/37.29	1.01/0.83
P2 (Push/Pull)	40.91/38.81	41.46/41.30	0.99/0.94
P3 (Push/Pull)	38.52/32.63	40.36/40.63	0.95/0.80
P4 (Push/Pull)	34.98/42.23	41.00/40.35	0.85/1.05
P5 (Push/Pull)	40.92/36.42	40.02/39.62	1.02/0.92
P6 (Push/Pull)	50.07/46.60	47.40/47.92	1.06/0.97

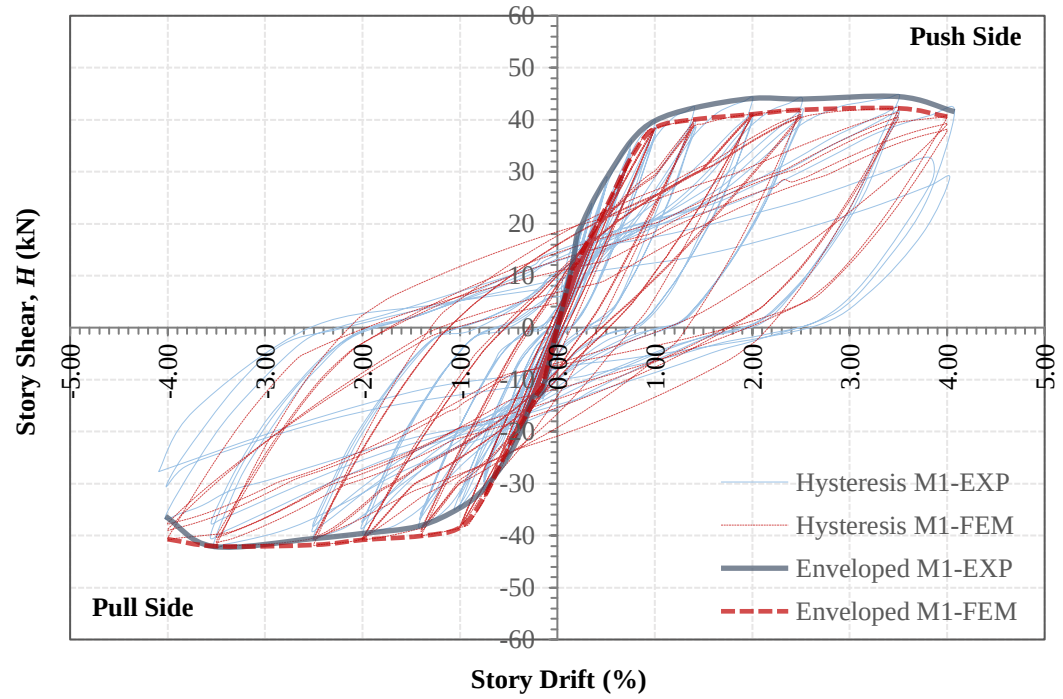

Figure 6.1 Comparison of hysteresis behavior between M1-FEM and M1-EXP

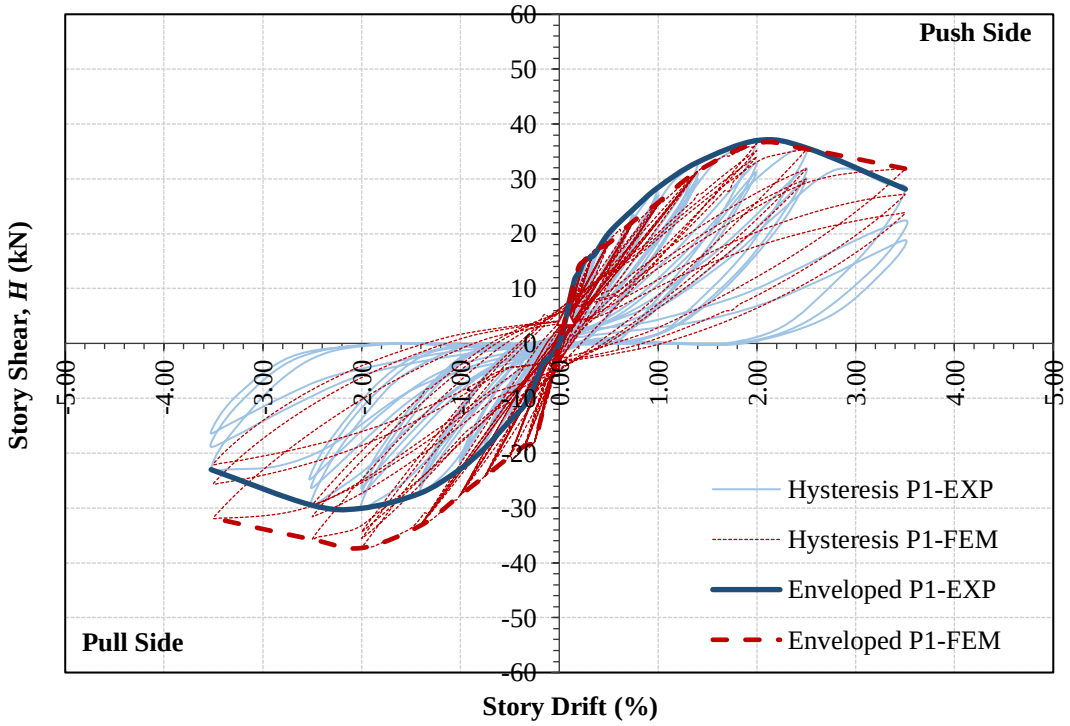

Figure 6.2 Comparison of hysteresis behavior between P1-FEM and P1-EXP

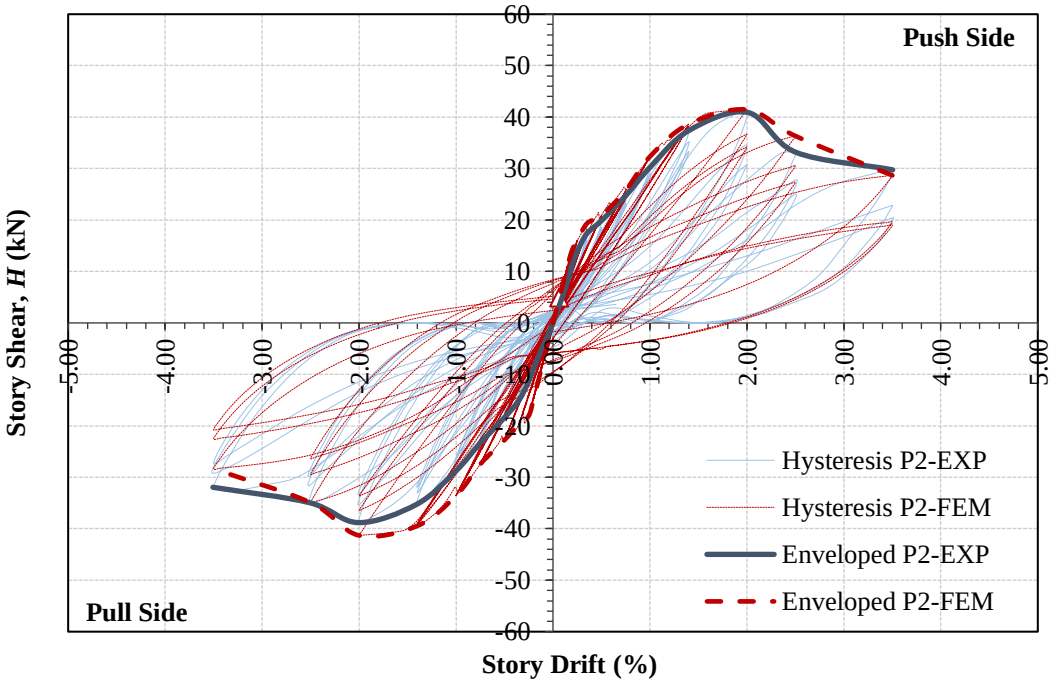

Figure 6.3 Comparison of hysteresis behavior between P2-FEM and P2-EXP

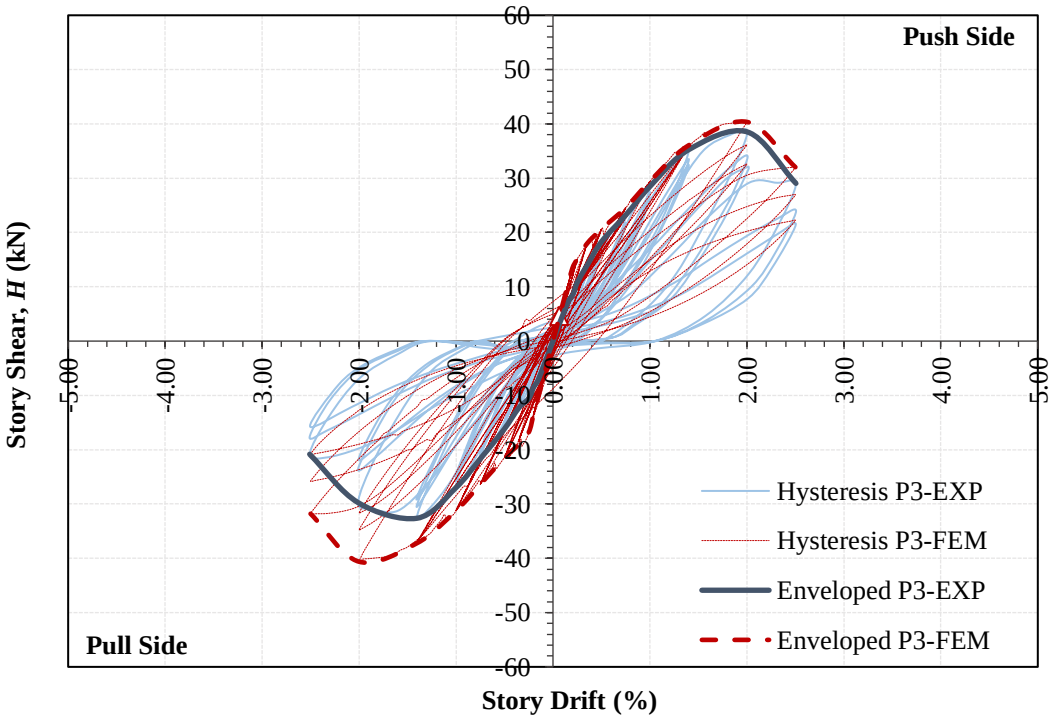

Figure 6.4 Comparison of hysteresis behavior between P3-FEM and P3-EXP

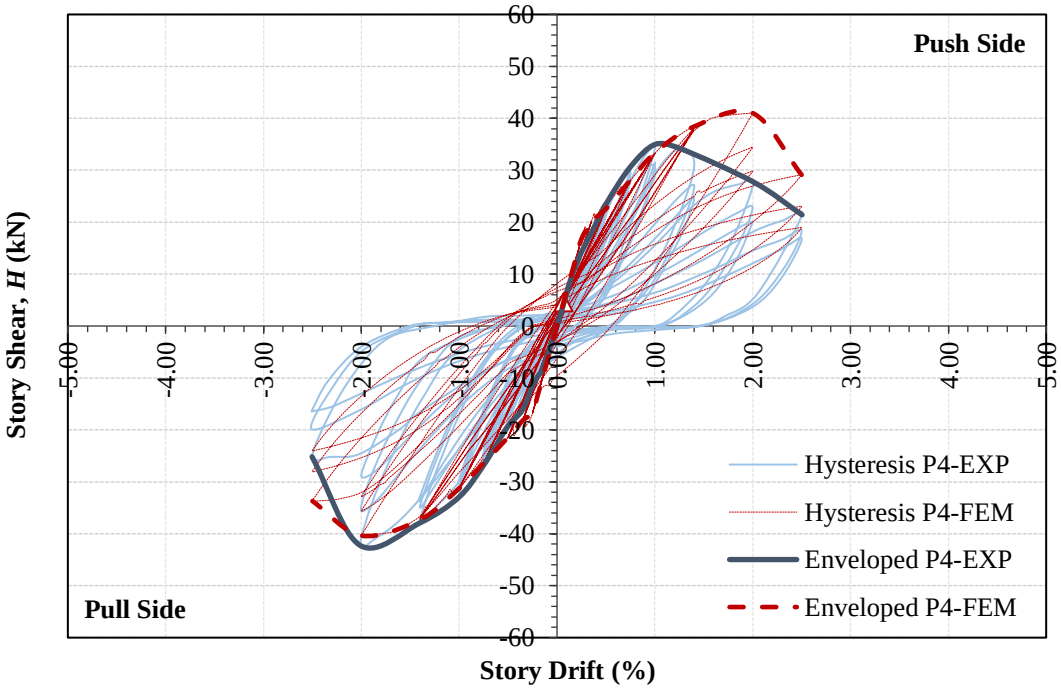

Figure 6.5 Comparison of hysteresis behavior between P4-FEM and P4-EXP

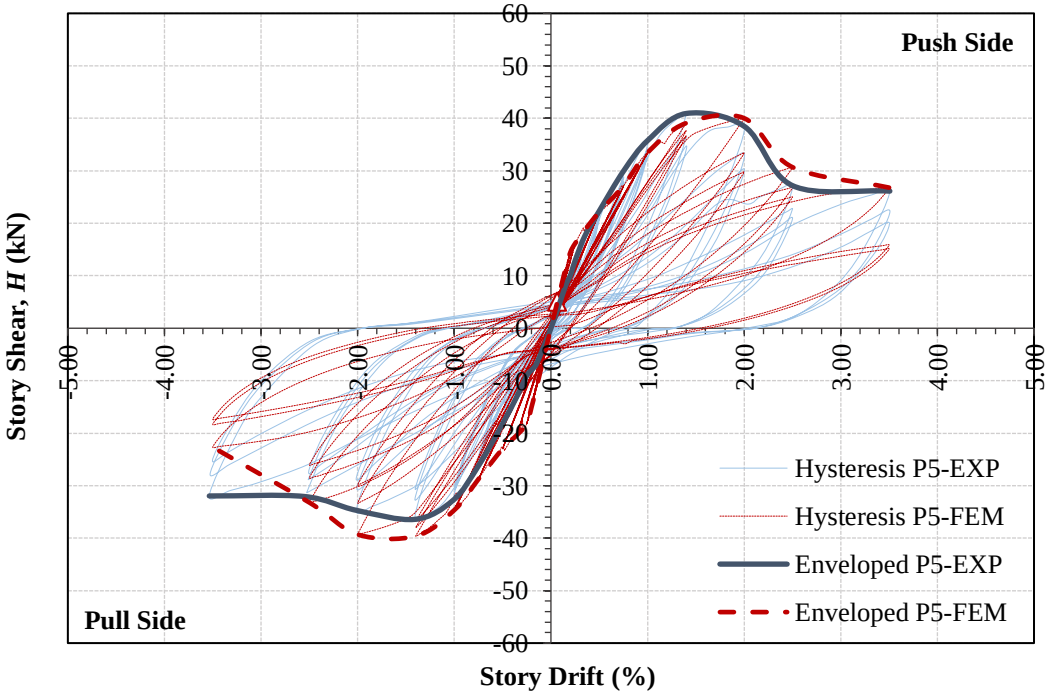

Figure 6.6 Comparison of hysteresis behavior between P5-FEM and P5-EXP

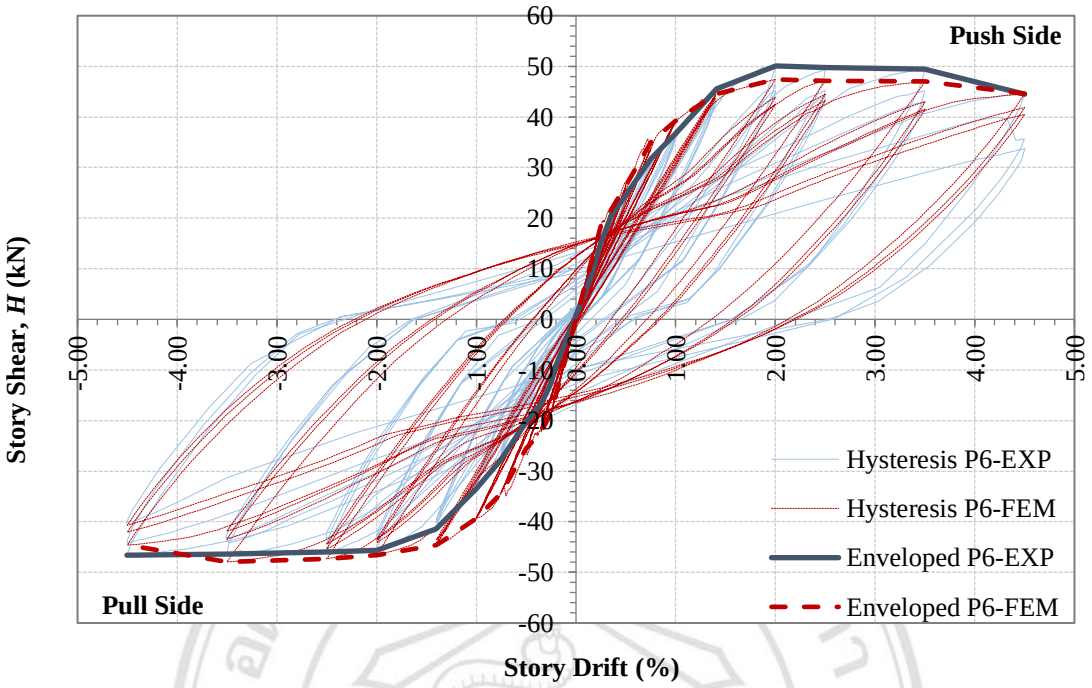

Figure 6.7 Comparison of hysteresis behavior between P6-FEM and P6-EXP

6.2 Parametric study on P-delta effect

6.2.1 Ultimate Strength with Variable Constant Column Load

The numerical backbone curves and the normalized backbone curves are shown in Figures 6.8 to 6.14 and Figures 6.15 to 6.21 respectively, for the monolithic (M) and precast (P) series. The analysis results of all series show that the ultimate decreased due to an increase of axial force value in the column elements. The increasing of column load led to additional secondary moment in addition to the primary bending moment. The numerical results of the maximum shear force (H_{avg}) by average of push and pull directions are shown in Table 6.2. The story shear capacity of the M-FEM progressively decreased for 5% - 12% from the first ($0.20f_c'A_g$) to the last ($0.50f_c'A_g$) in each 10% of column load increment. At the $0.50f_c'A_g$ column load level, the story shear is cumulatively dropped to 0.70 times of the story shear capacity at the $0.10f_c'A_g$ column load level.

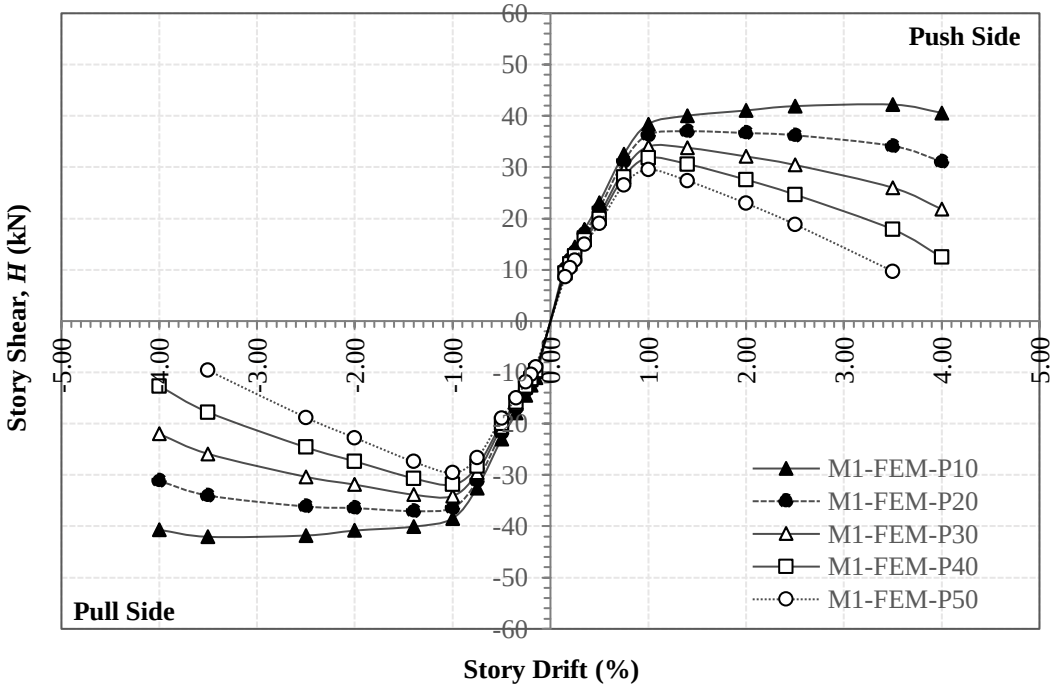

Figure 6.8 Numerical back bone curve of M1-FEM series

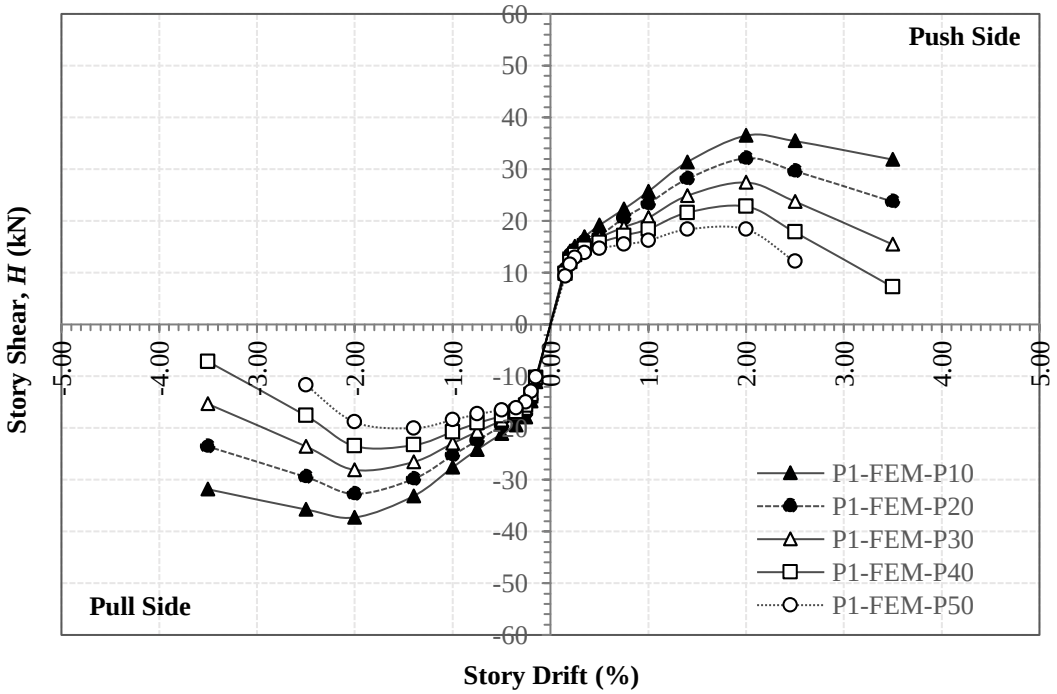

Figure 6.9 Numerical back bone curve of P1-FEM series

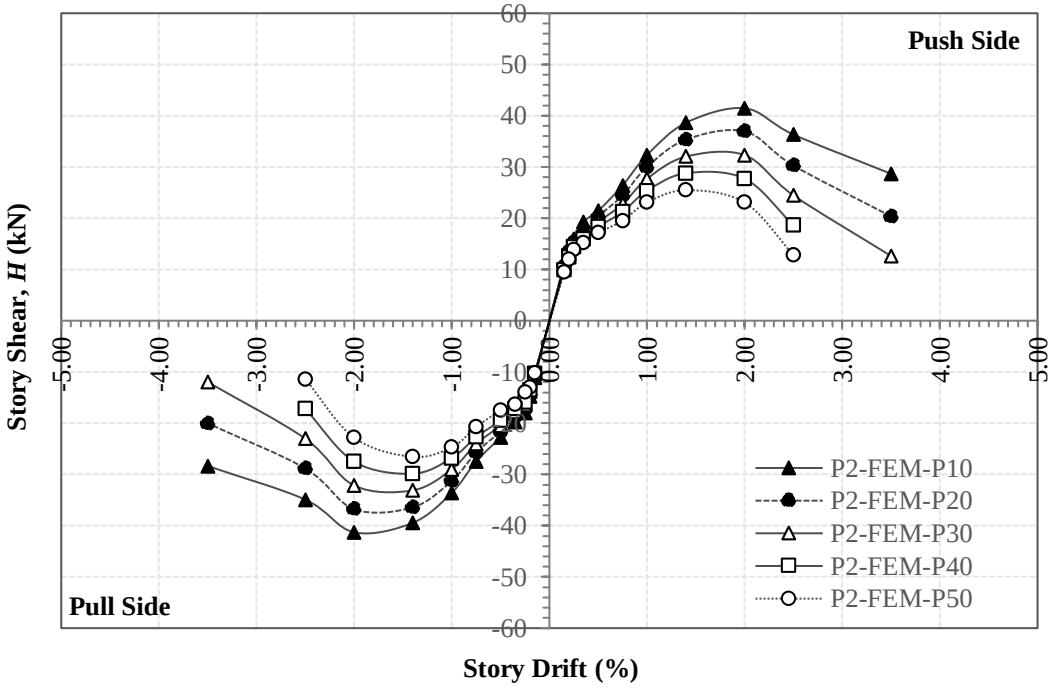

Figure 6.10 Numerical back bone curve of P2-FEM series

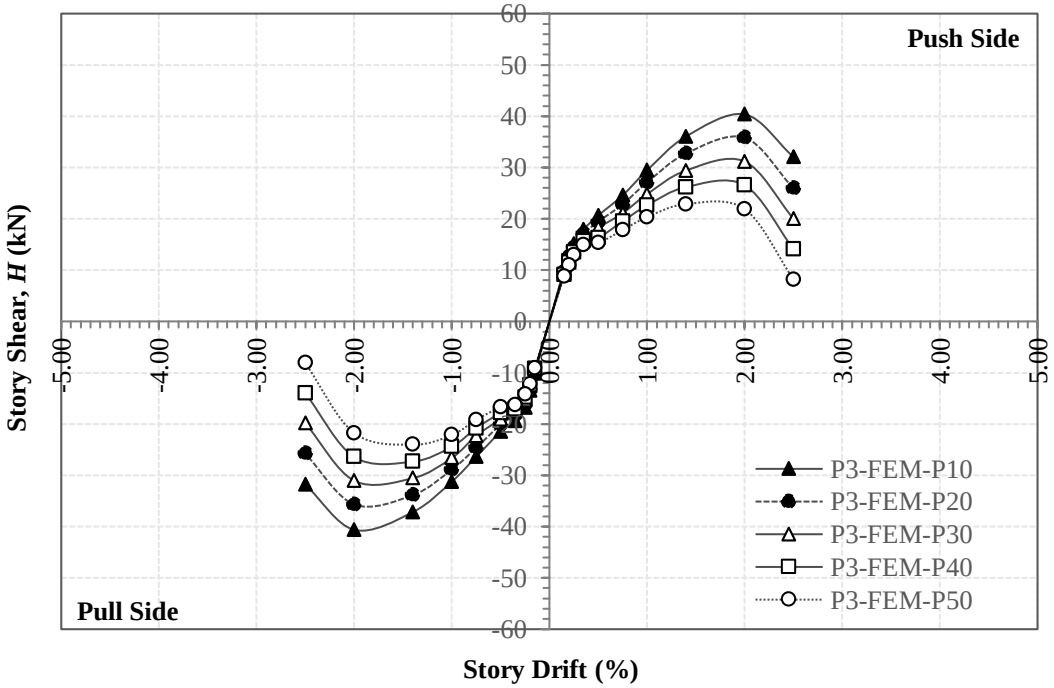

Figure 6.11 Numerical back bone curve of P3-FEM series

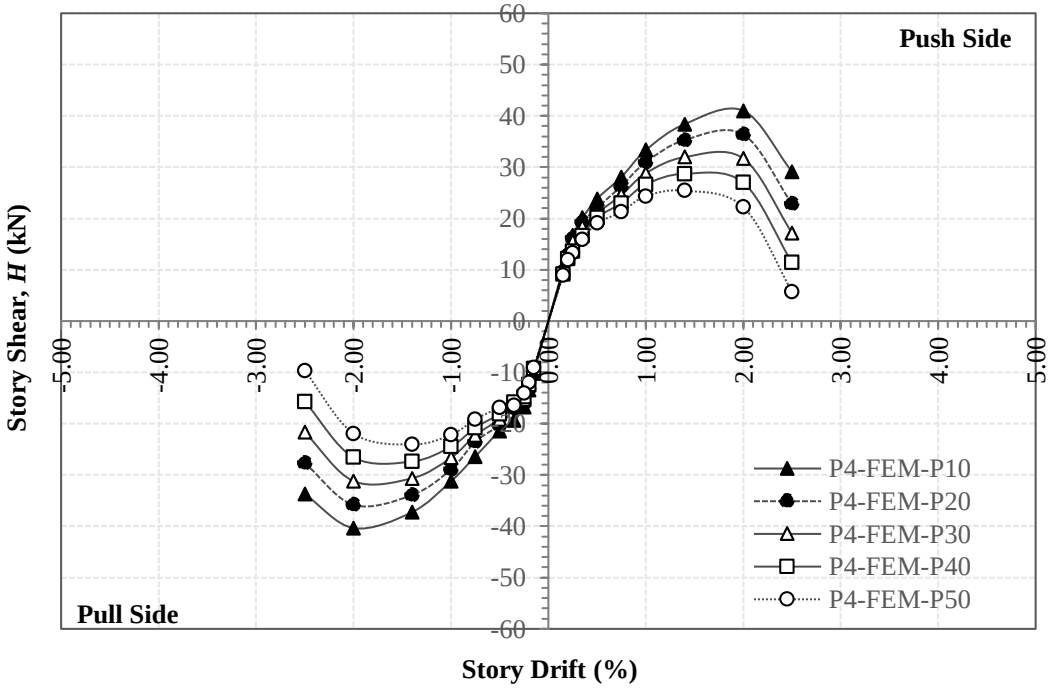

Figure 6.12 Numerical back bone curve of P4-FEM series

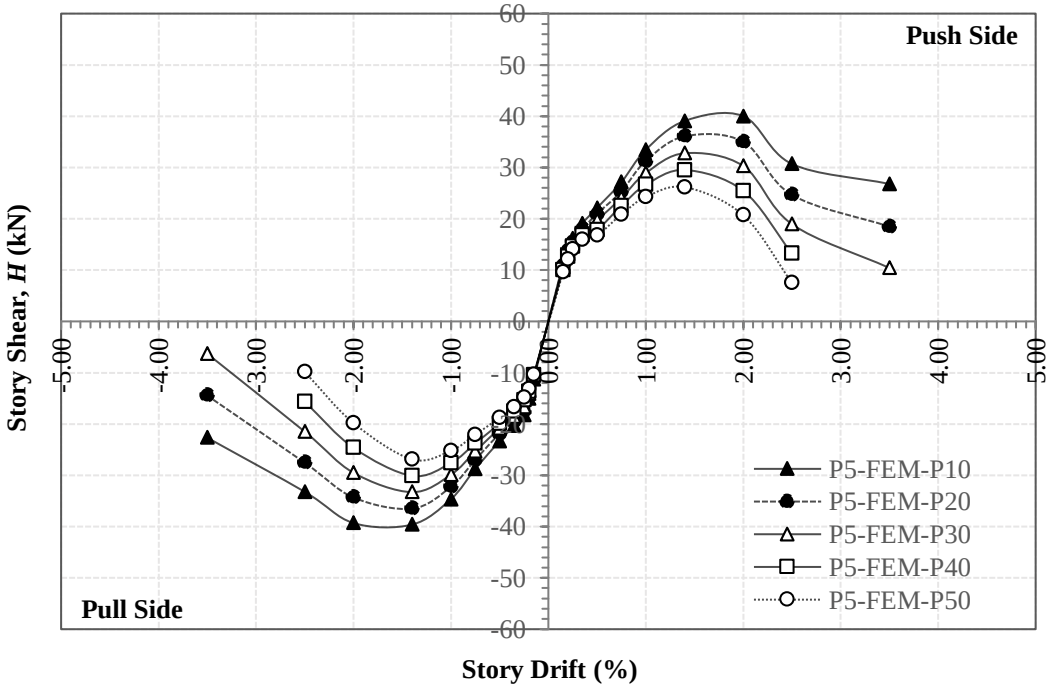

Figure 6.13 Numerical back bone curve of P5-FEM series

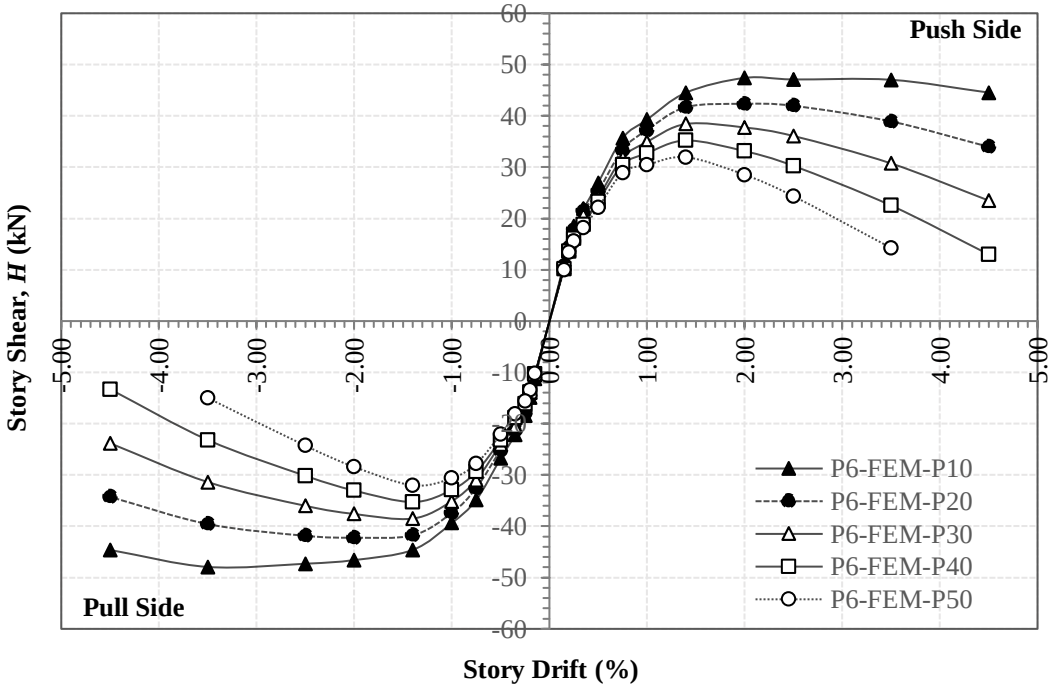

Figure 6.14 Numerical back bone curve of P6-FEM series

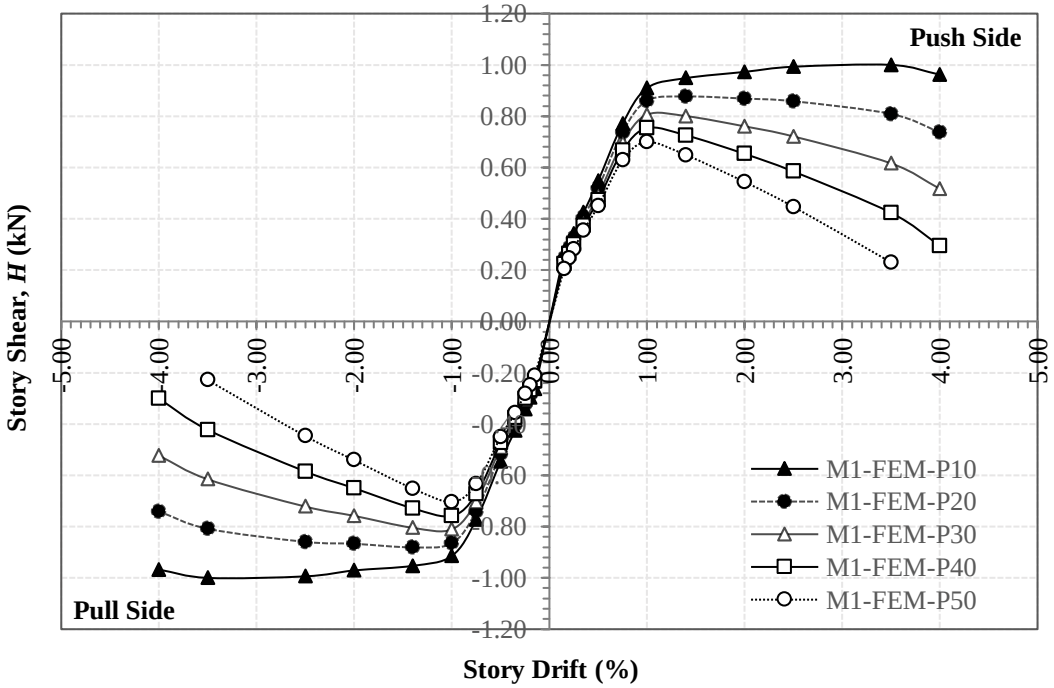

Figure 6.15 Normalized backbone curve of M1-FEM series

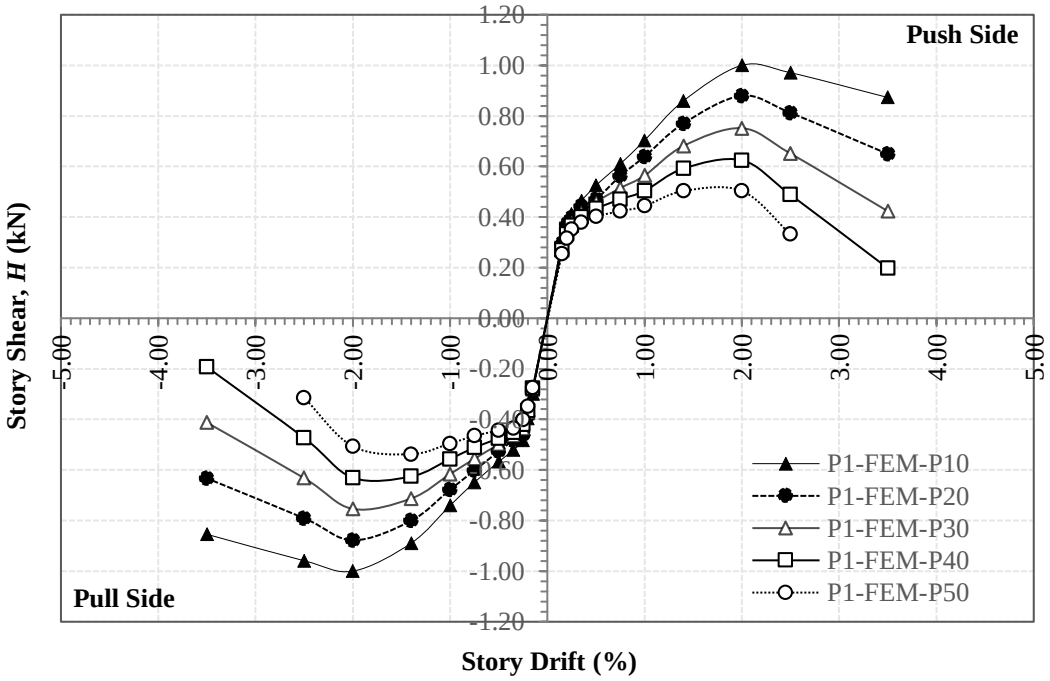

Figure 6.16 Normalized backbone curve of P1-FEM series

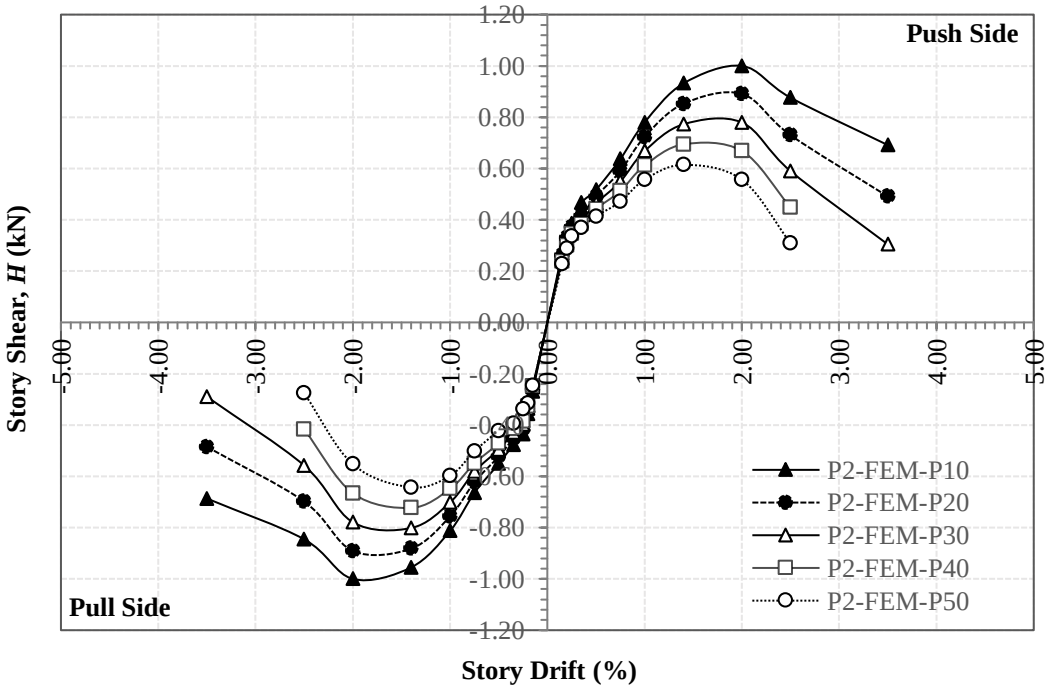

Figure 6.17 Normalized backbone curve of P2-FEM series

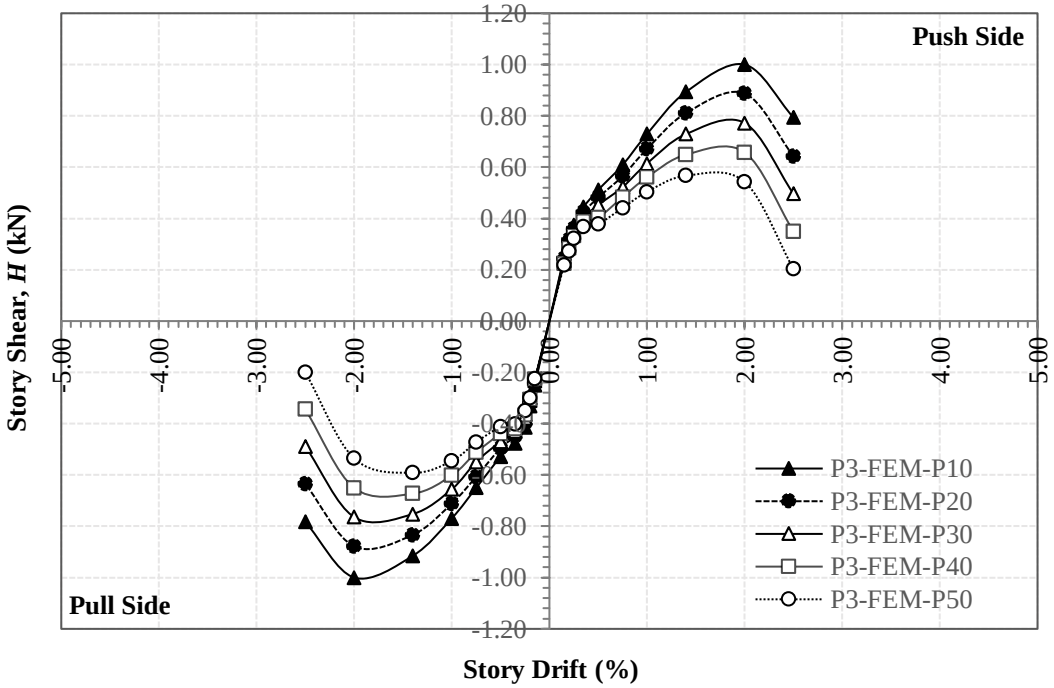

Figure 6.18 Normalized backbone curve of P3-FEM series

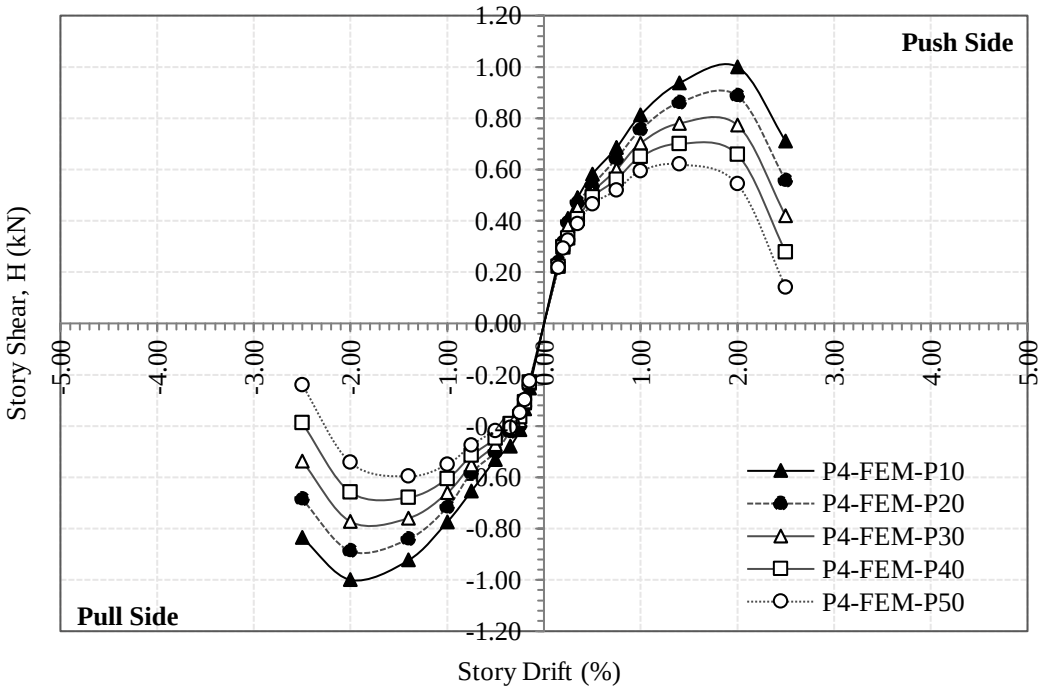

Figure 6.19 Normalized backbone curve of P4-FEM series

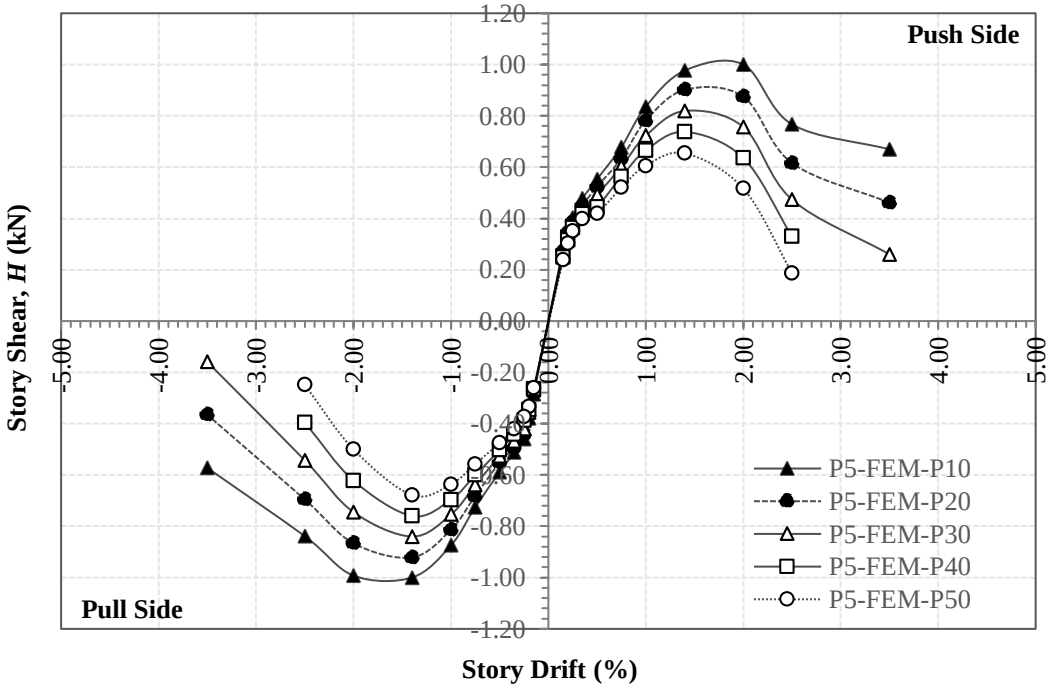

Figure 6.20 Normalized backbone curve of P5-FEM series

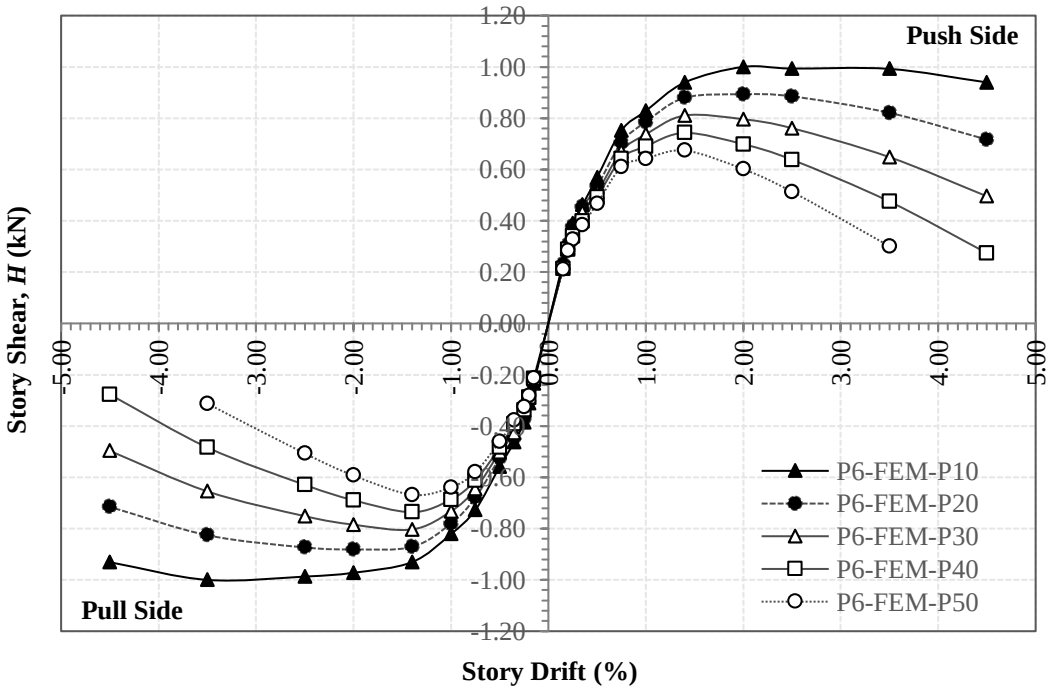

Figure 6.21 Normalized backbone curve of P6-FEM series

Table 6.2 Strength and story drift level at peak of story shear

FE Model	Maximum Strength (Push/Pull)		Average loading capacity (H_{avg}, kN)	Ratio of Average loading capacity $\left(\frac{H_{avg-P-xx}}{H_{avg-P-10}}\right)$	Rate of strength degradation	Cumulative rate of strength degradation
	Ultimate Load (kN)	Corresponding Story Drift (%)				
M1-FEM Series						
M1-FEM-P10	42.20/42.06	3.20/3.30	42.13	1.00	-	-
M1-FEM-P20	37.00/37.05	1.20/1.25	37.03	0.88	0.12	0.12
M1-FEM-P30	34.00/34.10	1.10/1.10	34.05	0.81	0.07	0.19
M1-FEM-P40	31.80/31.88	1.00/1.00	31.84	0.76	0.05	0.24
M1-FEM-P50	29.50/29.58	1.00/1.00	29.54	0.70	0.05	0.30
P1-FEM Series						
P1-FEM-P10	36.49/37.29	2.00/2.00	36.89	1.00	-	-
P1-FEM-P20	32.10/32.73	2.00/2.00	32.42	0.88	0.12	0.12
P1-FEM-P30	27.42/28.11	2.00/2.00	27.77	0.75	0.13	0.25
P1-FEM-P40	22.79/23.51	2.00/2.00	23.15	0.63	0.13	0.38
P1-FEM-P50	18.37/20.04	2.00/1.40	19.21	0.52	0.11	0.49
P2-FEM Series						
P2-FEM-P10	41.36/41.30	2.00/2.00	41.38	1.00	-	-
P2-FEM-P20	36.94/36.79	2.00/2.00	36.87	0.89	0.11	0.11
P2-FEM-P30	32.32/33.11	2.00/1.40	32.71	0.79	0.10	0.21
P2-FEM-P40	28.78/29.86	1.40/1.40	29.32	0.71	0.08	0.29
P2-FEM-P50	25.47/26.56	1.40/1.40	26.02	0.63	0.08	0.37
P3-FEM Series						
P3-FEM-P10	40.36/40.63	2.00/2.00	40.49	1.00	-	-
P3-FEM-P20	35.81/35.69	2.00/2.00	35.75	0.88	0.12	0.12
P3-FEM-P30	31.16/31.05	2.00/2.00	31.10	0.77	0.11	0.23
P3-FEM-P40	26.54/27.33	2.00/1.40	26.94	0.67	0.10	0.33
P3-FEM-P50	22.87/24.03	1.40/1.40	23.45	0.58	0.09	0.42
P4-FEM Series						
P4-FEM-P10	41.00/40.35	2.00/2.00	40.68	1.00	-	-
P4-FEM-P20	36.38/35.83	2.00/2.00	36.11	0.89	0.11	0.11
P4-FEM-P30	31.97/31.19	1.40/2.00	31.58	0.78	0.11	0.22
P4-FEM-P40	28.72/27.38	1.40/1.40	28.05	0.69	0.09	0.31
P4-FEM-P50	25.41/24.07	1.40/1.40	24.74	0.60	0.08	0.39
P5-FEM Series						
P5-FEM-P10	40.02/39.62	1.40/2.00	39.82	1.00	-	-
P5-FEM-P20	36.08/36.50	1.40/1.40	36.29	0.91	0.09	0.09
P5-FEM-P30	32.79/33.29	1.40/1.40	33.03	0.83	0.08	0.17
P5-FEM-P40	29.52/30.10	1.40/1.40	29.81	0.75	0.08	0.25
P5-FEM-P50	26.17/26.88	1.40/1.40	26.52	0.67	0.08	0.33
P6-FEM Series						
P6-FEM-P10	47.40/47.92	3.50/2.00	47.66	1.00	-	-
P6-FEM-P20	42.34/42.22	2.00/2.00	42.28	0.89	0.11	0.11
P6-FEM-P30	38.43/38.50	1.40/1.40	38.46	0.81	0.08	0.19
P6-FEM-P40	35.20/35.27	1.40/1.40	35.24	0.74	0.07	0.26
P6-FEM-P50	31.94/32.01	1.40/1.40	31.98	0.67	0.07	0.33

Regard to the numerical series of precast connections, the story shear deterioration of the P1-FEM series is severely. The maximum story shear at the column load level of

$0.50f_c'A_g$ is dropped by 0.49 times comparing to the $0.10f_c'A_g$ column loading. The lateral loading capacity degraded constantly about 10%-12% from every 10% increase in previous column load. For the P2-FEM, P3-FEM and P4-FEM series, the rates of strength degradation are around 8%-12% of previous maximum strength in each 10% increment of column load. At the $0.50f_c'A_g$ column load, the shear capacities dropped significant to around 0.58-0.63 times against maximum strength at the level of $0.10f_c'A_g$ column load. For the P5-FEM and P6-FEM series, the rates of strength degradation and cumulative rate of strength degradation are very similar. The shear strength of both FEM series at the $0.50f_c'A_g$ column load are equal to 0.67 times of loading capacity at a level of axial column load equal to $0.10fc'A_g$.

It can be conclude that the P5 and P6 precast connections for relocating plastic beam hinge are very similar with the monolithic connection in terms of strength deterioration at the high column loading. Otherwise, high level of strength deterioration at the high level of carried column load is observed in the other precast connection due to the major failure mode as bonding failure at the potential plastic hinging zone, especially the precast P1 connection.

6.2.2 Numerical Ductility

Table 6.3 shows the numerical ductility factor from the FE predictions. The simulation results indicated that the FE models with lower axial column load possessed greater displacement ductility. In regards to backbone curves predictions, there were no significant strength drops in the M1-FEM-P10 and P6-FEM-P10 model. This pattern is mimicked by that of the experimental results while the other models are evidenced after the yield points.

Table 6.3 Comparison of numerical displacement ductility factor

FE model	Push Side			Pull Side			μ_{avg}
	Δ_u (%)	Δ_y (%)	μ	Δ_u (%)	Δ_y (%)	μ	
M1-FEM-P10	4.00	1.00	4.00	4.00	1.00	4.00	4.00
M1-FEM-P20	4.00	0.87	4.60	3.90	0.87	4.48	4.54
M1-FEM-P30	2.75	0.83	3.25	2.72	0.85	3.20	3.25
M1-FEM-P40	2.10	0.82	2.56	2.05	0.82	2.50	2.53
M1-FEM-P50	1.75	0.78	2.24	1.70	0.80	2.13	2.18
P1-FEM-P10	3.50	1.50	2.33	3.40	1.40	2.43	2.38
P1-FEM-P20	2.97	1.38	2.15	2.70	1.27	2.13	2.14
P1-FEM-P30	2.55	1.32	1.93	2.40	1.08	2.22	2.08
P1-FEM-P40	2.35	1.12	2.10	2.30	0.77	2.99	2.54
P1-FEM-P50	2.22	0.56	3.96	2.20	0.33	6.67	5.32
P2-FEM-P10	2.70	1.28	2.11	2.45	1.20	2.04	2.08
P2-FEM-P20	2.38	1.20	1.98	2.40	1.18	2.03	2.01
P2-FEM-P30	2.26	1.10	2.05	2.15	1.09	1.97	2.01
P2-FEM-P40	2.20	1.04	2.11	2.15	1.00	2.15	2.13
P2-FEM-P50	2.10	1.03	2.03	2.09	0.92	2.27	2.16
P3-FEM-P10	2.35	1.42	1.65	2.38	1.30	1.83	1.74
P3-FEM-P20	2.30	1.33	1.74	2.30	1.18	1.96	1.85
P3-FEM-P30	2.25	1.25	1.80	2.20	1.13	1.96	1.88
P3-FEM-P40	2.18	1.10	1.98	2.15	1.00	2.15	2.07
P3-FEM-P50	2.10	1.00	2.10	2.05	0.95	2.16	2.13
P4-FEM-P10	2.28	1.20	1.90	2.40	1.22	1.97	1.93
P4-FEM-P20	2.20	1.10	2.00	2.26	1.18	1.92	1.96
P4-FEM-P30	2.17	1.00	2.17	2.16	1.10	1.96	2.07
P4-FEM-P40	2.10	0.86	2.44	2.08	1.00	2.08	2.26
P4-FEM-P50	2.00	0.60	3.33	2.10	0.80	2.63	2.98
P5-FEM-P10	2.29	1.15	1.99	2.44	1.05	2.32	2.16
P5-FEM-P20	2.20	1.10	2.00	2.26	1.00	2.26	2.13
P5-FEM-P30	2.13	1.00	2.13	2.10	0.95	2.21	2.17
P5-FEM-P40	2.03	0.93	2.18	2.00	0.85	2.35	2.27
P5-FEM-P50	1.85	0.89	2.08	1.80	0.75	2.40	2.24
P6-FEM-P10	4.50	1.00	4.50	4.50	1.10	4.09	4.30
P6-FEM-P20	4.10	0.91	4.51	4.20	1.00	4.20	4.35
P6-FEM-P30	3.75	0.84	3.75	3.20	0.90	3.56	3.65
P6-FEM-P40	3.15	0.80	3.15	2.42	0.88	2.75	2.95
P6-FEM-P50	2.93	0.75	2.93	2.20	0.80	2.75	2.84

6.2.3 Stability index

Stability is a major problem of seismic structure in nonlinear behavior. A study of Paulay (1979) proposed a stability index considering the secondary order *P-Δ* effect with post-yield lateral displacement. A basic formula had been adopted to explain the stability criterion, which is the ratio of the *P-Δ* moment to the lateral mechanism moment as shown in equation (6.1). This is similar to the stability indices developed by other studies (ACI318-14 2014, Paulay 1978). The index suggests that if the ratio of the secondary moment to the ideal primary moment of a subframe exceeds 0.15, the *P-Δ* effect is a

necessary consideration. As the inelastic behavior is very common under a real earthquake, Paulay and Priestley (1992) proposed a study on a modified stability index (Q^*) to consider an inelastic displacement as shown in equation (6.2). The inelastic approach is utilized where the modified index exceeds a limit state of 0.085.

$$Q = \frac{P\Delta_y}{Hh} \tag{6.1}$$

$$Q^* = (\mu + 0.5)\frac{P\Delta_y}{Hh} = (\mu + 0.5)Q \tag{6.2}$$

Where Q is elastic stability index, Q^* is a modified stability index, P is the sum of gravity load carrying on top column (for multiple story building), Δ_y is the yield lateral deflection due to H, H is the lateral shear, μ is the displacement ductility factor, h is the column height (2,260 mm, in the study).

As shown in Table 6.3, the elastic and modified stability indices were calculated from *Eq.6.1* and 6.2 respectively. It can be seen that the numerical results for the elastic stability indices of FE models excepting P1-FEM series with lower 20% of column capacities were not exceeded 0.15, unnecessary consideration of the P-Δ effect. For the P1-FEM series, the P-Δ effect consideration should be necessary if the carried column load is greater than 10% of column capacities due to the elastic stability index exceeds a limit state of 0.15. The elastic indices of P6-FEM series were lower than the other precast FEM series. In other words, the P1- FEM series were highest in terms of the elastic stability indices in every value of column load. From the reason, it can be revealed that the P6 precast connection was the best performance for stability consideration.

The numerical results in the modified stability indices of all FE models exceeded 0.085. For this reason, the secondary order should be considered even though the corresponding displacements were in an elastic region. Moreover, both stability indices increased following the values of the axial column load. In conclusion, the stability of the subframe not only depended on a maximum ductility, but it also depended on the carried load.

Table 6.4 Comparison of elastic stability index and modified stability index

FE model	Average		α Factor of axial load	P (kN)	H_{avg} (kN)	Q	Q^*
	Δ_y (%)	μ					
M1-FEM-P10	1.00	4.00	0.10	235	42.13	0.06	0.25
M1-FEM-P20	0.87	4.48	0.20	470	37.03	0.11	0.55
M1-FEM-P30	0.84	3.20	0.30	705	34.05	0.17	0.64
M1-FEM-P40	0.82	2.50	0.40	940	31.84	0.24	0.73
M1-FEM-P50	0.79	2.13	0.50	1,175	29.54	0.31	0.83
P1-FEM-P10	1.45	2.43	0.10	235	36.89	0.09	0.27
P1-FEM-P20	1.33	2.13	0.20	470	32.42	0.19	0.51
P1-FEM-P30	1.20	2.22	0.30	705	27.77	0.30	0.83
P1-FEM-P40	0.95	2.99	0.40	940	23.15	0.38	1.34
P1-FEM-P50	0.45	6.67	0.50	1,175	19.21	0.27	1.95
P2-FEM-P10	1.24	2.04	0.10	235	41.38	0.07	0.18
P2-FEM-P20	1.19	2.03	0.20	470	36.87	0.15	0.38
P2-FEM-P30	1.10	1.97	0.30	705	32.71	0.24	0.58
P2-FEM-P40	1.02	2.15	0.40	940	29.32	0.33	0.87
P2-FEM-P50	0.98	2.27	0.50	1,175	26.02	0.44	1.22
P3-FEM-P10	1.36	1.83	0.10	235	40.49	0.08	0.18
P3-FEM-P20	1.26	1.96	0.20	470	35.75	0.16	0.41
P3-FEM-P30	1.19	1.96	0.30	705	31.10	0.27	0.66
P3-FEM-P40	1.05	2.15	0.40	940	26.94	0.37	0.97
P3-FEM-P50	0.98	2.16	0.50	1,175	23.45	0.49	1.30
P4-FEM-P10	1.21	1.97	0.10	235	40.68	0.07	0.17
P4-FEM-P20	1.14	1.92	0.20	470	36.11	0.15	0.36
P4-FEM-P30	1.05	1.96	0.30	705	31.58	0.23	0.58
P4-FEM-P40	0.93	2.08	0.40	940	28.05	0.31	0.80
P4-FEM-P50	0.70	2.63	0.50	1,175	24.74	0.33	1.04
P5-FEM-P10	1.10	2.32	0.10	235	39.82	0.06	0.18
P5-FEM-P20	1.05	2.26	0.20	470	36.29	0.14	0.38
P5-FEM-P30	0.98	2.21	0.30	705	33.03	0.21	0.56
P5-FEM-P40	0.89	2.35	0.40	940	29.81	0.28	0.80
P5-FEM-P50	0.82	2.40	0.50	1,175	26.52	0.36	1.05
P6-FEM-P10	1.05	4.09	0.10	235	47.66	0.05	0.24
P6-FEM-P20	0.96	4.20	0.20	470	42.28	0.11	0.50
P6-FEM-P30	0.87	3.56	0.30	705	38.46	0.16	0.65
P6-FEM-P40	0.84	2.75	0.40	940	35.24	0.22	0.73
P6-FEM-P50	0.78	2.75	0.50	1,175	31.98	0.28	0.93